

Indicators of plume constituents from HICOTM

Nicholas Tuffillaro and Curtiss O. Davis

College of Oceanic and Atmospheric Science, Oregon State University, USA.

Katherine B. Jones

Department of Chemistry, University of Otago, New Zealand.

SUMMARY

Littoral river plumes are complex optical environments. To begin to resolve this complexity we use hyperspectral data, and an extension of ‘dark pixel correction’ methods (Chavez 1988), to produce radiance maps that allow us to distinguish different constituents in the water column ranging from glacial rich sediments (silica’s) to muds and algae. We present data from two sites: the Columbia River in the Northwest of the United States, and the Otago Shelf fed by the Clutha River on the South Island of New Zealand. For this study the instrument used to collect data was HICO (Corson 2010; Davis et. al. 2010) — the Hyperspectral Imager for the Coastal Ocean — developed by the United States Naval Research Lab (NRL) and currently flying on the International Space Station. HICO has 90 channels between 400-900 nm and a ground sampling distance of 90 m. These early results illustrate how space borne hyperspectral imaging can enhance our view of the suspended matter in river plumes along a coast.

INTRODUCTION

Ideally, accurate physics based atmospheric correction is used to obtain surface remote sensing reflectance, and estimates of the inherent optical properties (IOP’s) of the top of the water column, from a space borne at-sensor radiance (Gordon and Wang 1994). The IOP’s, in turn, can be used to estimate the constituents of the water column from models and simulations of the scattering and absorption properties of the specific constituents of coastal waters (Lee 2006).

In many applications, however, such as identifying different types and sources of suspended matter in the upper water column, understanding qualitative mixing patterns, or providing operational guidance for in field sampling, a calibrated radiance image (without atmospheric correction) of a scene may suffice. For instance, the Fluorescence Line Height method (FLH), using the 709 MERIS channel, is proving to be a good indicator of coastal algal blooms (Gower et. al. 2005; King et. al. 2010), and is helpful in both their initial detection, and also providing guidance for field sampling (Tuffillaro et. al. 2010). Additionally, Gower and co-workers have advocated working directly from the Level 1b (L1) data lacking atmospheric correction in estimating FLH, especially in near coastal waters. The FLH maps from L1 data are often used to indicate a specific water constituent, and not to accurately estimate the concentration. That is, FLH is often used to ‘indicate’ the presence of high concentrations of algae, relative to surrounding waters.

We will use the term ‘indicator map’ to denote a radiance or reflectance image of a scene, which like, the L1 FLH products, are usually computed from the calibrated at-sensor radiance and are meant to highlight specific constituents of the water column, but not necessarily provide a calibrated measurement or concentration. Because we are simply after indicators, rather than estimates of concentrations, we make more liberal use of scene based empirical methods to go directly from L1 data to an ‘indicator’ for a specific water constituent.

We view these indicator maps as, in some sense, an extension of line height methods, made possible by the use of hyperspectral data which allows us get a finer look at the suspended matter constituents of coastal waters. In line height methods, adjacent channels are used to develop indicators for a product which is relatively insensitive to atmospheric effects because of the proximity in wavelength of the channels utilized. In the method described here our intent is the same. That is, we want to develop indicators that are relatively insensitive to atmospheric effects, but can also make use of spectral data over a wider wavelength range, and not just adjacent channels. We emphasize that this approach is made possible because of the relatively dense channel sampling provided by hyperspectral data, which allows us to identify features in the spectra that can be used as indicators for specific types of suspended matter. In order to facilitate operational use and adaptability to different scenes, our initial approach relies on an empirical model for ‘dark water pixels’ that is easily tuned for different regions.

Alternatively, as we move away from Line Height Methods we move toward band-ratio methods. So the method described here might also prove useful simple preprocessing procedure for band-ratio methods, or point us toward an extension of band-ratio methods that allows us to experiment with both the location and spectral widths of the bands in order to create an indicator for a target product.

In either case, as we move from space-borne multispectral to hyperspectral remote sensing data, we expect that the additional spectral channels will find use both in scene based atmospheric correction methods (Lee et. al. 2007), as well as developing a more complete collection of indicators of the constituents of coastal waters.

DARK PIXEL MODEL

The starting point for atmospheric correction of a sensor above water radiance, $L_{\mathcal{T}}$, is the decomposition,

$$L_{\mathcal{T}}(\lambda) = L_a(\lambda) + \mathcal{T}(\lambda)L_w(\lambda), \quad (1)$$

where L_a accounts for atmospheric and sea-surface reflection, L_w picks up contributions below the water surface, and \mathcal{T} denotes the transmittance from the water surface to sensor (Gao et. al. 2000).

In developing ‘indicator maps,’ we will consider a slightly different decomposition. Namely, we start by imagining, at every pixel, the at sensor radiance we would see if the water was clear, a so-called dark water pixel. This is an ‘idealized’ quantity, but the difference between this ideal radiance signal, and the observed signal at sensor, provides information about what is in the water, which is relatively independent of what is in the atmosphere. Thus it is a good starting point for creating an ‘indicator’ function for what is in the water.

In our approach a dark water pixel will be defined ‘empirically,’ based on an image, or collection of images, of a region of interest, and choosing pixels, or patches of pixels, which determine ‘dark water,’ or water free of river plume materials, or other features of interest, for that region. So in practice, the dark water pixel could contain some background material in the water column that we will consider as ‘clear water,’ or a ‘dark pixel,’ which is typical for the region. We could call this type of pixel, which contains some below water signal, a regional dark pixel, but in the following discussion we will just call it a dark pixel. It is the background signal from which we start any further signal processing.

Mathematically we can write this decomposition as:

$$L_{\mathcal{T}}(\lambda) = L_a(\lambda) + \mathcal{T}(\lambda)(L_d(\lambda) + L_b(\lambda)), \quad (2)$$

$$= L_M(\lambda) + L_I(\lambda), \quad (3)$$

where L_M is the modeled spectrum, and L_I is the ‘indicator’ spectrum, it is simply the residual between the at sensor radiance minus any modeling we do for the spectrum. If L_M is simply chosen as a dark pixel in the scene than it is what is normally referred to as ‘dark pixel subtraction’, a very simple but often effective scheme for atmospheric correction (Chavez 1988). The terms $L_d(\lambda)$ and $L_b(\lambda)$ are called the ‘dark water’ and ‘bright water’ contributions to $L_w(\lambda)$ respectively.

The trick to this approach is finding (a probably empirical) model of dark pixel spectra that allow us to create a data based decompositions of $L_T(\lambda)$ to identify one or more dynamic water constituents of interest. To find such a model we start by examining an image from HICOTM of the at-sensor radiance (L1B) for a typical dark water scene, in this case the waters around Midway Atoll (Fig. 1).

To create an empirical model to fit the ‘dark water’ pixels shown by the circles in Fig. 1 we take a guess at the following functional form:

$$L_m(\lambda) = (a + b(\lambda - \lambda_1))^{-4} \quad (4)$$

where a and b are model parameters which are to be estimated from the spectral data — λ_n and $L_m(\lambda_n)$ — and λ_1 is the first value of the wavelength in data set being modeled — a constant. In HICO L1B data sets, each at-sensor pixel consists 90 radiance values between about 0.4 nm to 0.95 nm. The typical swath size covers approximately 42 km by 190 km, and 500 by 2000 pixels. To ‘model’ the data we limit our data sets to wavelengths between 0.45 nm to 0.95 nm, so in our data sets $\lambda_1 = 0.45$ nm and $\lambda_N = 0.95$ nm.

The choice of window of wavelengths is deliberate for our modeling. First, we want a functional form which will fit the data well, but not too well — that is we want to deliberately ‘smooth’ the data by imposing a model that has only a few — in this case two — free parameters. This ‘smoothing’ process will, for instance, average over atmospheric absorption features, but these features can prove useful in building indicator functions. For dark pixels, the wavelength window chosen is dominated by a decaying trend in both incoming solar irradiance and Rayleigh scattering. In particular, λ_1 is chosen at approximately the maximum of solar irradiance over the wavelengths considered so that — on average — the function we are trying to estimate is monotonically decreasing with wavelength. Second, we need a window which also covers information useful for both dark pixels (whose shape is dominated by Rayleigh scattering between 0.45 nm to 0.7 nm) and bright pixels which can have significant radiance past 0.7 nm.

The functional form for the model does not exhibit fourth order scaling per se, rather the use of two constants effectively introduces terms in a functional expansion that also includes modeling terms of order λ^{-4} , λ^{-3} , ..., λ^0 . So it is more proper to say that the model has a leading term that has an inverse fourth order power.

As Figure 1 illustrates, the functional form approximates the dark pixel data well with just two parameters in wavelengths considered. The actual functional fit is achieved with a nonlinear least squares optimization procedure (Dennis 1977). Critical for any nonlinear optimization is the ‘initialization’ of the seed values. The empirical dark pixel model presented in Eq. (4) is easy to initialize. To find the starting values for our nonlinear optimization — (a_0, b_0) — we algebraically solve Eq. (4) for two different values. Choosing the first spectral point in the HICO data set, (λ_1, L_1) , we find a

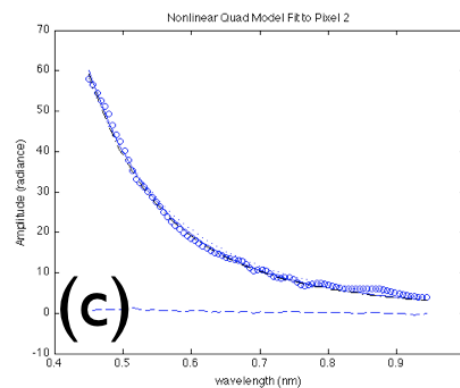
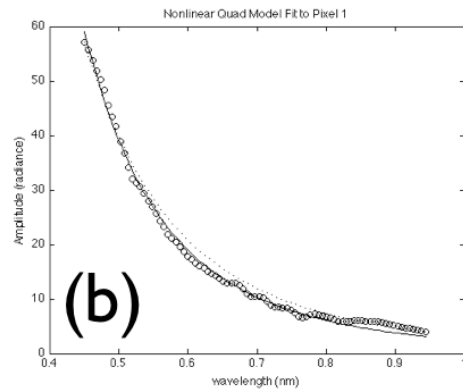
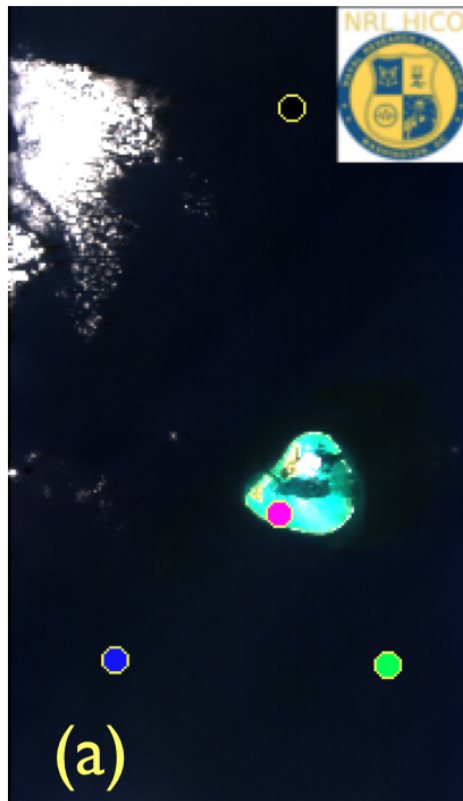


Figure 1: *Image of Midway Atoll and selected spectra at indicated points – (a) HICO RGB image from 25 March 2010. Bright circles indicate regions for the spectra shown in Fig. 1 (b). The black, blue, and green dots indicate regions we expect to see ‘typical’ dark pixel spectra — i.e. clear water spectrum’s. The magenta dot indicates an example of a (very) bright spectrum. The image is composed from at-sensor radiances, LIB data is supplied by NRL’s HICOTM team [Corson 2010]. (b) At-sensor radiance for black pixel in Fig. 1 (a). The raw data is indicated by circles. The initialization for the nonlinear fit is shown by the dashed line. The final nonlinear fit to the dark pixel empirical model is shown by the solid line. (c) At-sensor radiance for blue pixel in Fig. 1 (a). The lower line shows the difference with the black pixel in Fig. 1 (b).*

seed value for a as $a_0 = L_1^{-4}$, and this in turn can be used to compute b_0 at any other spectral value. In our case we chose the end point, $\lambda_N = 0.95$ nm, with $b_0 = (L_N^{-4} - a_0)/(\lambda_N - \lambda_1)$. The specific values for the data shown in Fig. 2 are $(a_0, b_0) = (0.36, 0.71)$, and after optimization $(a, b) = (0.36, 0.79)$. Computing optimized values for (a, b) across different ‘dark water pixels’ in a scene provides a measure of the variation of the model and data. As Figure 3 illustrates, they do not change much in the Midway scene, typically the values for (a, b) vary by less than 5%.

EXMAPLES: OTAGO SHELF AND COLUMBIA RIVER

Moving to more complex waters we consider coastal flow along the Otago shelf on the South Island New Zealand. The flow along the Otago shelf is steered Northward by the Southland current. 75 km south of Dunedin, Broadbay, and the biologically productive Otago Peninsula, is the Clutha River. A major source of freshwater input, the Clutha is glacier fed from thr Southern Alps and is rich in silicates, which produces very bright coastal waters (Pfannkuche 2002). The Clutha is the highest volume river in New Zealand, discharging a mean flow of $614 m^3/s$ The Taieri River, about 30 km south of Broadbay, is more sediment rich, and both rivers provide many of the nutrients of the biologically rich Otago shelf coastal waters. A HICO image of the waters along the Otago Shelf is shown in Fig. 2.

The spectra at the points indicated in Figure 2(a) is shown in Figure 2(c). Pixel 1, black, is meant to sample dark waters. Indeed, the dark pixel model works well for this spectral data with optimization values of $(a, b) = (0.4, 0.84)$. The blue pixel is taken near the mouth of the Taieri, and the magenta pixel near the mouth of the Clutha. The silica rich waters of the Clutha appear to increase the water brightness between 0.6nm and 0.75 nm relative to the the Taieri.

It would be interesting to distinguish the (silica rich) Clutha and (sediment rich) Taieri waters based on remote remote sensing data. To attempt this we decompose the L1B spectrum by applying the dark pixel model on pixel by pixel basis. We then present the ‘residual’ spectrum, the L1B radiance spectra, minus the estimated L_M . An image based on the L_I , indicator spectrum, is shown in Figure 2(b). In this case our ‘indicator function’ is simply a choice of RGB channels which highlights the spectra between 0.6 nm and 0.7 nm, making the Clutha waters bright blue relative to the greenish Taieri waters in Figure 2(b). In-situ data from bi-monthly cruises are currently being collected eastward from Broadbay. Some initial match-ups are shown in Figure 2(d).

As a second example we take a look at the mouth of the Columbia river in the Northwest of the United States. The L1B HICO RGB image from 19 March 2010 is shown in Figure 3(a). After an examination of the spectra, we choose a channel at about 540 nm to attempt to highlight sediment in these waters. The spectra for L_I for this channel is shown in Figure 3(b). Images from the summer (July 8-13), spectra and sediment indicator maps are shown in Fig. 3(c-f). We are currently trying to match-up these type of data with in-situ sediment records for the Columbia.

CONCLUSION

We describe a method for separation of hyperspectral L1 data into a ‘dark water pixel,’ and residual portion. We suggest that, particularly in cases where atmospheric correction is problematic, the construction of indicators based on the residual spectrum can be useful in distinguishing different types of class 2 waters. An examination of the residual spectrum, for a few well chosen pixels in a

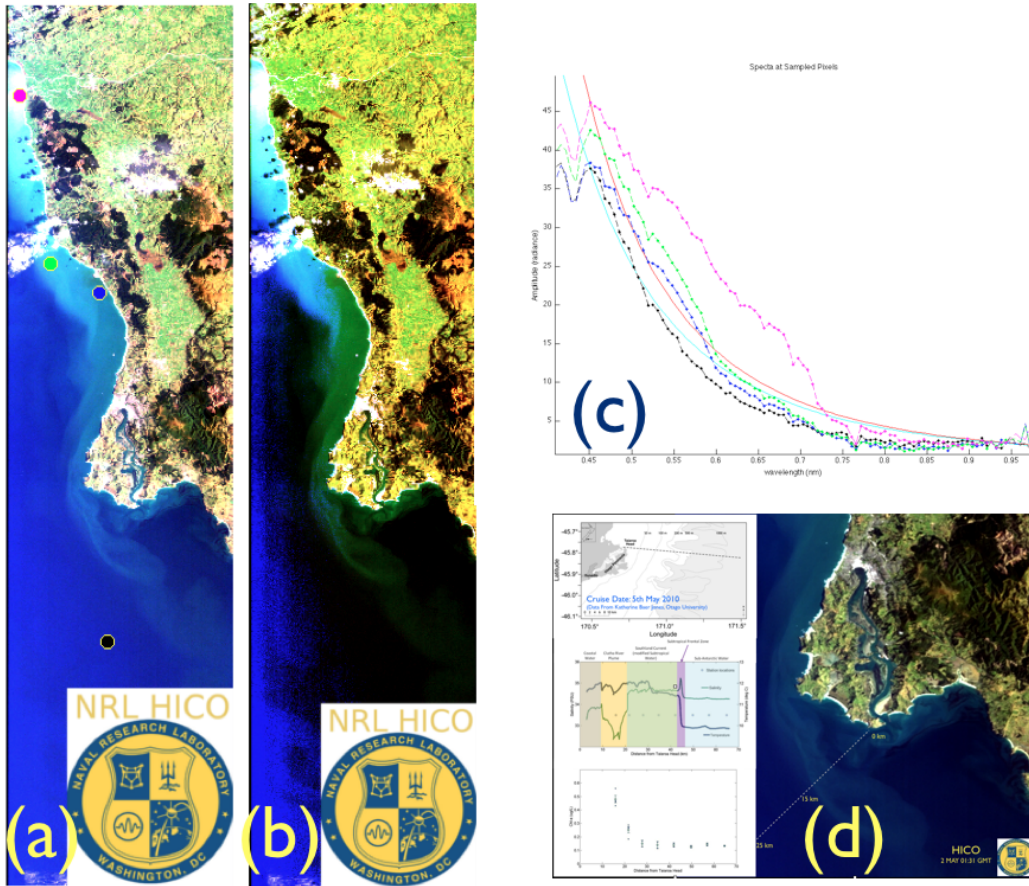


Figure 2: Image of Otago Shelf waters with indicator map, spectra, and examples of in-situ data: (a) LIB HICO image of the Clutha to Broadbay, New Zealand, 2 May 2010. The bright water covers 70 km from the mighty Clutha (top, south) to Broadbay (bottom, north). (c) LIB Radiance spectrum of pixels on the Otago shelf indicated in Fig. 2(a). Black spectra — dark water, Blue — near the Taieri mouth, and Magenta — near the Clutha mouth. (b) HICO image constructed from L_1 spectrum of the Otago shelf waters. The Clutha waters (blue) are distinguished from the Taieri waters (green). (d) In-situ cruise data for water properties for 5 May 2010 eastward from Talarona Head, transecting the Otago shelf coastal waters.

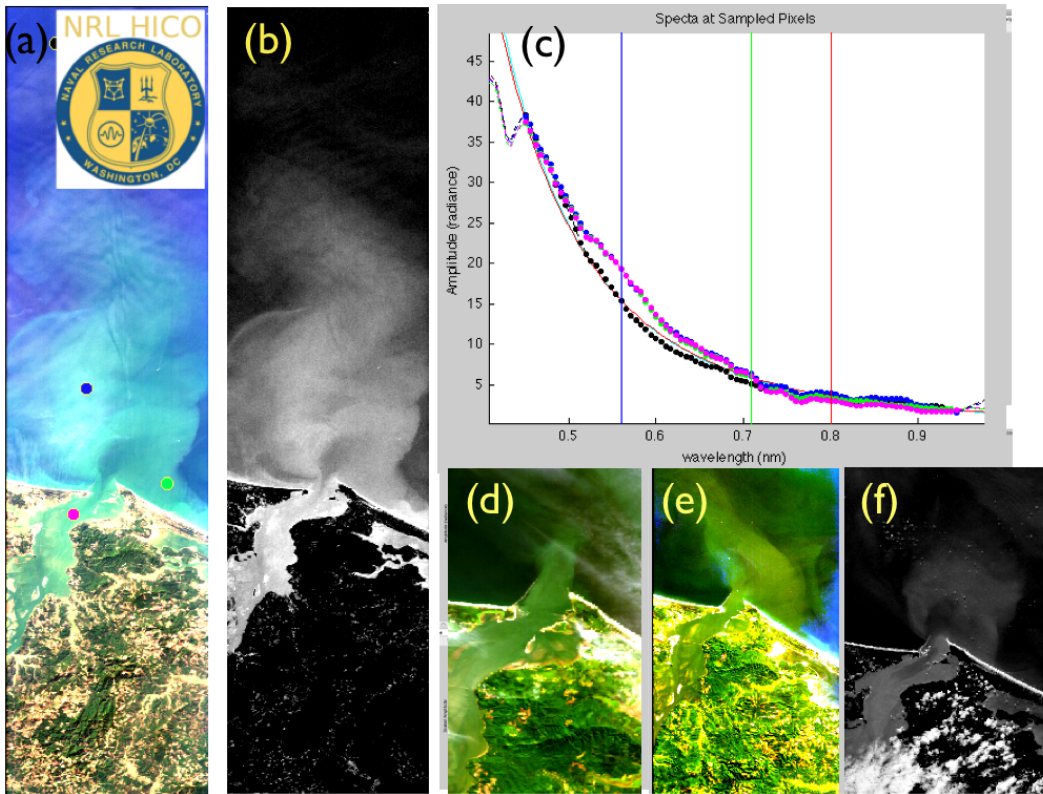


Figure 3: Images of Columbia River with indicator map highlighting sediments: (a) LIB HICO image of Columbia River mouth 19 March 2010. (b) An indicator for sediments in the Columbia River based on the the dark pixel spectral separation for the image presented in Fig. 3(a). (c-f) Typical spectra and sediment indicator maps for July 2010.

scene, is often enough to suggest channels that can be useful in building indicator maps to highlight or reveal the presence of waters with significantly different suspended materials. We illustrate the idea with silica rich, and sediment rich, bright coastal waters off the Otago shelf, and also present initial work on the analysis of sediment rich waters surrounding the Columbia River mouth.

ACKNOWLEDGEMENTS

We greatly appreciate the support from our sponsors. We thank the HICO™ team at NRL for building the spectrometer and coordinating its operation on the ISS, and providing calibrated HICO™ data for academic research. We also thank Jasmine Nahomiak at Oregon State University for setting up the academic distribution portal for HICO™ data.

REFERENCES

- Chavez, P. S. Jr. (1988). An improved dark-object subtraction technique for atmospheric scattering correction of multispectral data, *Remote Sensing Environ.*, 24, pp. 459-279.
- Corson, Michael (2010). The hyperspectral imager for the coastal ocean: Littoral environmental characterization from the international space station, *Ocean Optics XX*, Abstract #132.
- Davis, Curtiss, Arnone, Robert, Gould Rick, Corson, Michael, and Lee, Zhong-Ping (2010) , The hyperspectral imager for the coastal ocean (HICO) provides a new view of the coastal ocean, *Ocean Optics XX* Abstract #193.
- Dennis, J.E. (1977). *Nonlinear Least Squares: State of the Art in Numerical Analysis*, ed. D. Jacobs, Academic Press, pp. 269-312.
- Gao, B. C., M. J. Montes, Z. Ahmad, and C. O. Davis (2000). Atmospheric correction algorithm for hyperspectral remote sensing of ocean color from space, *Applied Optics*, **36** (6) p. 887-896.
- Gordon, H. R. and M. Wang (1994). Retrieval of water leaving radiances and aerosol optical thickness over the oceans with SeaWiFS: a preliminary algorithm, *Appl. Opt.* **33** 443-452.
- Gower, J., S. King, G. Borstad and L. Brown (2005), Detection of intense plankton blooms using the 709nm band of the MERIS imaging spectrometer, *Int. J. of Remote Sensing*, **26** (9): 2005-2012.
- King, S. A., Gower J. F. (2010). Satellite remote sensing of the spring bloom in coastal waters of British Columbia, 2010 Ocean Sciences Meeting Abstract BO24A-07 (2010).
- Lee, ZhongPing (ed.) (2006). *Remote sensing of inherent optical properties: Fundamentals, tests of algorithms, and applications*, IOCCG Report Number 5, (2006).
- Lee, ZhongPing, B. Casey. R. A. Arone, A. D. Weidemann, M. J. Montes, B-C Gao, W. Goode, C. O. Davis, and J. Dye (2007). Water and bottom properties of a coastal environment derived from Hyperion data measured from the EO-1 spacecraft platform, SPIE DOI: 10.1117/12.791119.
- Pfannkuche, J. (2002) Optical properties of Otago shelf waters: South Island New Zealand, *Estuarine, Coastal and Shelf Science*, **55** (4), 613-627.
- Tufillaro, N., C. O. Davis, Z-P Lee (2010). Comparison of MERIS and HICO spectral imaging along the Oregon Coast, 2010 Ocean Sciences Meeting Abstract IT31A-07.